Global Phase Locking and Multi-Scale Resonance Mapping: A Unified Framework for Quantum Communication, Interconnects, Imaging, and Metrology

Pingxin Wang
LFR Resonance Systems Ltd
info@lfrfrequency.com

Abstract

We propose a unifying framework for four key domains in quantum technology—communication/computation, integrated interconnects, imaging/packaging, and metrology/standards—based on *global phase locking* (GPL) and *multi-scale resonance mapping* (MSRM). This approach shifts the focus from state replication to network-wide phase coherence, offering experimentally verifiable witnesses and scalable design principles.

1 Introduction

Quantum communication, interconnects, imaging, and metrology face a shared bottleneck: maintaining coherence across heterogeneous scales. Rather than pursuing state duplication (limited by the No-Cloning theorem [1]), we suggest embedding all nodes into a *common phase manifold*. This reorientation provides a natural route to scalability, robustness, and standardization across platforms.

2 Core Model: Global Phase Locking

Phase dynamics of node j follow a Kuramoto-type model:

$$\dot{\theta}_j = \omega_j + \sum_k K_{jk} \sin(\theta_k - \theta_j) + \xi_j(t), \tag{1}$$

where ω_j are natural frequencies, K_{jk} are couplings (engineerable across scales), and ξ_j captures phase noise. A sufficient locking threshold is

$$K_j^{\text{eff}} = \sum_k K_{jk} > |\Delta_j|, \tag{2}$$

ensuring each node converges to the shared phase frame. The order parameter,

$$R(t) = \frac{1}{N} \sum_{j=1}^{N} e^{i\theta_j(t)}, \tag{3}$$

quantifies global coherence, with $|R| \to 1$ indicating phase-locked collective dynamics. Noise-limited error bounds can be expressed as

$$\mathbb{E}[e_j^2] \lesssim \frac{D_{\phi,j}}{K_j^{\text{eff}}}. \tag{4}$$

3 Applications Across Domains

3.1 Communication and Computation

In quantum networks, distributing identical quantum states is constrained by the no-cloning theorem. Under a global phase-locking framework, information can instead be embedded as phase trajectories shared across all nodes. This allows network-wide coherence without state duplication, providing a scalable mechanism for secure communication and distributed computation.

3.2 Integrated Circuits and Interconnects

As device complexity scales, cumulative phase noise and cross-talk in interconnects limit performance. By employing hierarchical synchronization—first on-chip, then across modules, and finally system-wide—the effective coupling suppresses detuning at each level. This reduces resource overhead and enables scaling without exponential error growth. Locking time approximately follows

$$T_{\text{lock}} \sim (K^{\text{eff}})^{-\alpha}, \quad \alpha \approx 1. \tag{5}$$

3.3 Imaging and Packaging

Dissipative engineering can be harnessed to passively draw local modes into a global phase frame, stabilizing collective behaviour. The collective output is quantified by

$$P(t) = \left| \sum_j A_j e^{i\theta_j(t)} \right|^2, \tag{6}$$

with normalized efficiency

$$\eta(t) = \frac{P(t) - \sum_j A_j^2}{(\sum_j A_j)^2 - \sum_j A_j^2} \in [0, 1]. \tag{7}$$

3.4 Metrology and Standards

A global phase reference can serve as a quantum benchmark. Cross-node correlations provide experimental witnesses:

$$C_{jk} = \langle a_j^\dagger a_k \rangle, \tag{8}$$

with $\arg C_{jk}$ converging to a common value across platforms.

4 Multi-Scale Resonance Mapping

To unify heterogeneous scales $\{\Omega_s\}$, we define a global resonance representative:

$$\Omega^\star = \arg\min_{\Omega} \sum_{s=1}^{L} w_s \, d(\Omega, \Omega_s), \tag{9}$$

where d is a frequency or phase cost function, and w_s are scale-dependent weights.

5 Simulation Results

Numerical simulations confirm that once the effective coupling exceeds the detuning/noise scale, systems converge to global phase coherence. These results illustrate both the threshold behaviour and robustness of the proposed framework, providing experimentally accessible witnesses (order parameter, power, efficiency) that can validate global phase locking across heterogeneous quantum systems. In practice, such quantities are measurable: $|R(t)|$ can be inferred from cross-correlation of homodyne signals, $P(t)$ corresponds to detected output power, and $\eta(t)$ can be calibrated as the normalized collection efficiency.

6 Conclusion

This work introduces a unified framework—Global Phase Locking (GPL) combined with Multi-Scale Resonance Mapping (MSRM). Simulation results support synchronization thresholds and efficiency gains, while proposed observables (order parameters, correlation matrices, normalized efficiency) are experimentally accessible with homodyne detection, power readout, and efficiency calibration, strengthening the pathway from model to implementation.

References

[1] Wootters W K and Zurek W H 1982 *Nature* **299** 802–803

[2] Nielsen M A and Chuang I L 2000 *Quantum Computation and Quantum Information* (Cambridge Univ. Press)

[3] Kuramoto Y 1975 *Lecture Notes in Physics* **39** 420–422

[4] Strogatz S H 2000 *Physica D* **143** 1–20

[5] Acebrón J A *et al.* 2005 *Rev. Mod. Phys.* **77** 137–185

[6] Poyatos J F, Cirac J I and Zoller P 1996 *Phys. Rev. Lett.* **77** 4728

[7] Mari A *et al.* 2013 *Phys. Rev. Lett.* **111** 103605

[8] Walter S, Nunnenkamp A and Bruder C 2014 *Phys. Rev. Lett.* **112** 094102

[9] Gill P 2005 *Metrologia* **42** S125–S137

[10] Ludlow A D *et al.* 2015 *Rev. Mod. Phys.* **87** 637–701

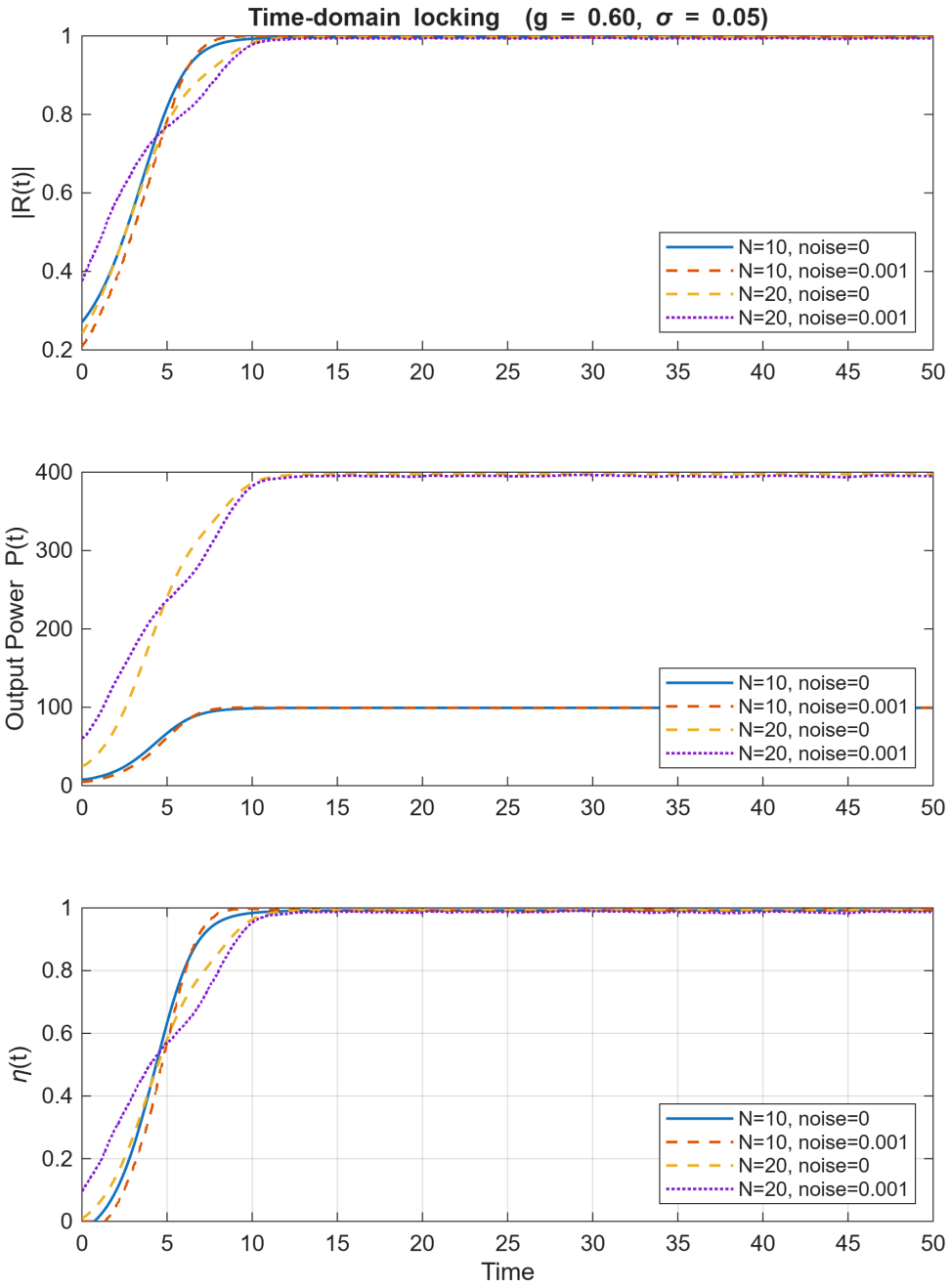

Figure 1: Time-domain dynamics: $|R(t)|$ (top), output power $P(t)$ (middle), and normalized efficiency $\eta(t)$ (bottom); comparisons for different N and noise levels.

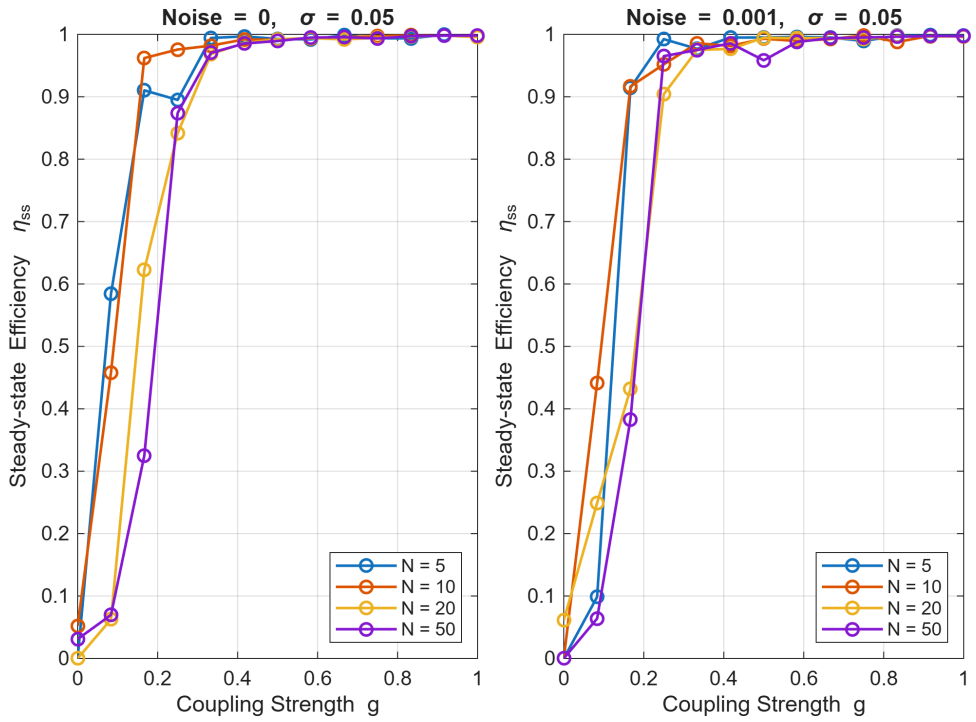

Figure 2: Steady-state efficiency η_{ss} vs coupling strength g for varying N. A clear synchronization threshold and noise robustness are observed.